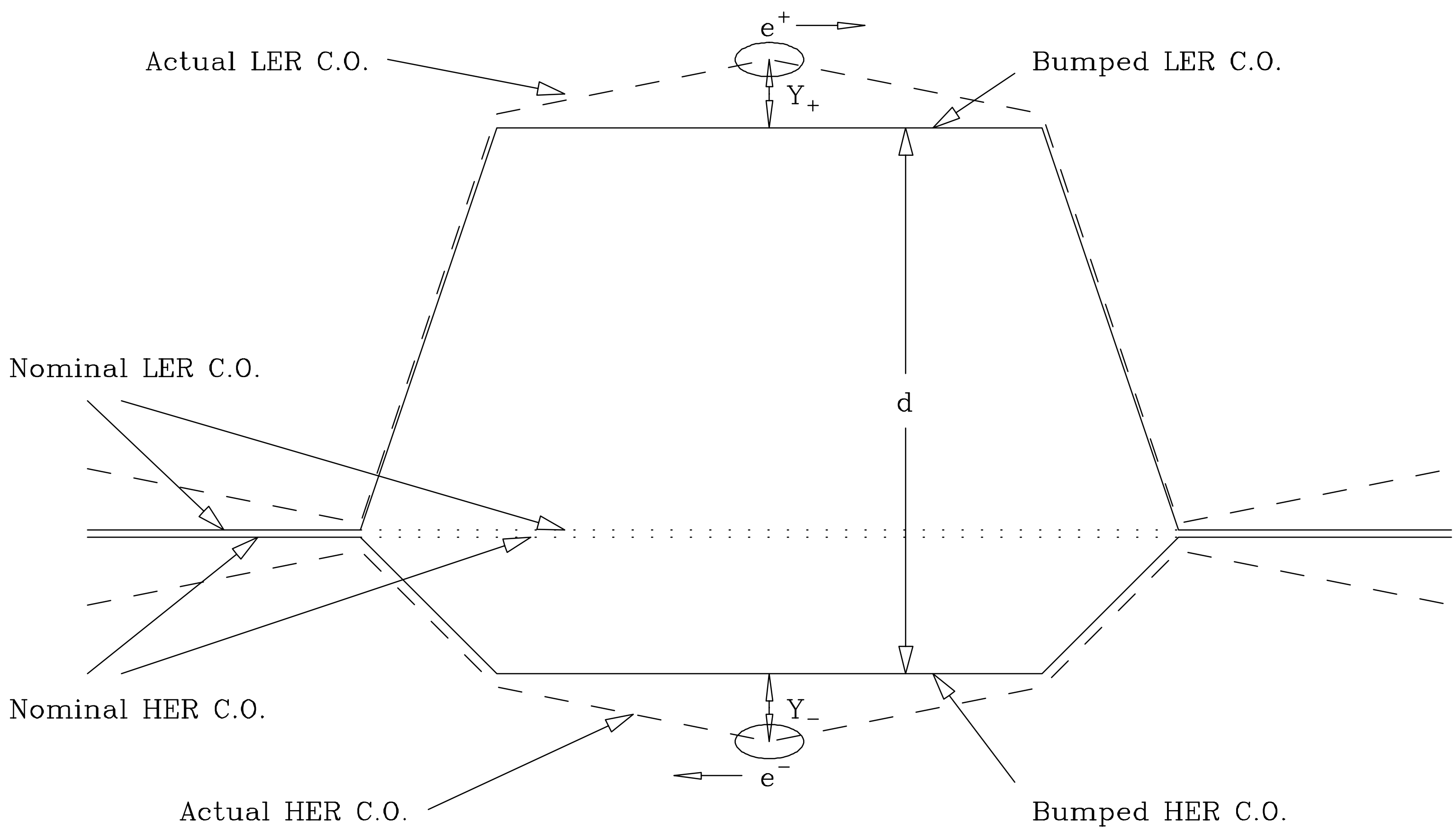

Fig. 1. Elevation sketch of the closed vertical orbit bump in the immediate vicinity of the IP. The nominal closed orbits (C.O.) are indicated by the horizontal solid and dotted lines (shown slightly displaced for the sake of clarity). The two bunches are shown on their actual orbits, displaced by Y_+ and Y_- from their bumped orbits. In this case $Y_+>0$ and $Y_-<0$, so that the actual beam separation is $d+Y_+-Y_-$. The deflections $\Delta Y'_+$ and $\Delta Y'_-$ are <0 and >0, respectively.

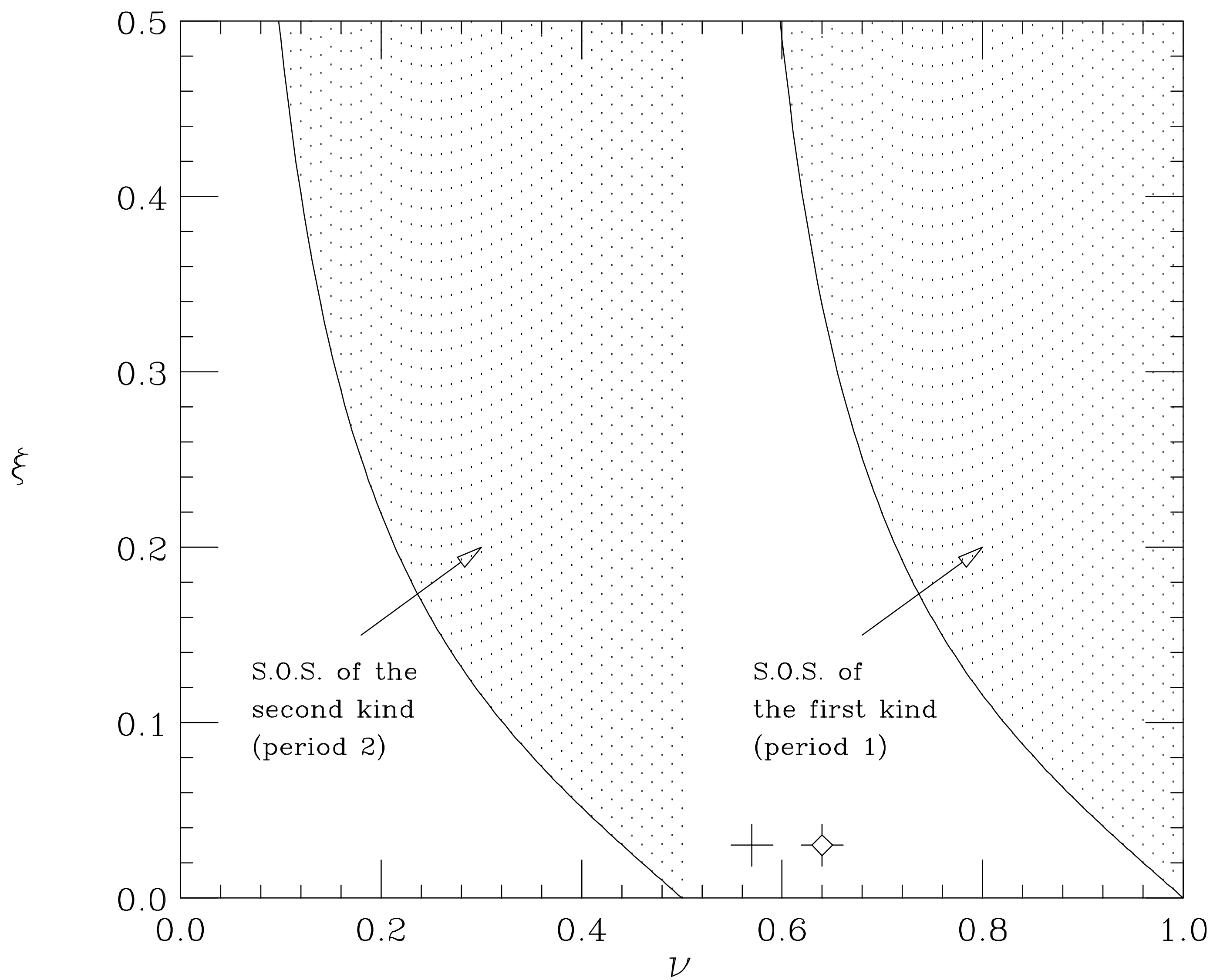

Fig. 2. The shaded domains define the areas of spontaneous orbit separation (S.O.S.) The crosses indicate the operating points for APIARY 7.5 (ν_x=0.64, ν_y=0.57, ξ_x=ξ_y=0.03), both safely away from the undesirable regions.

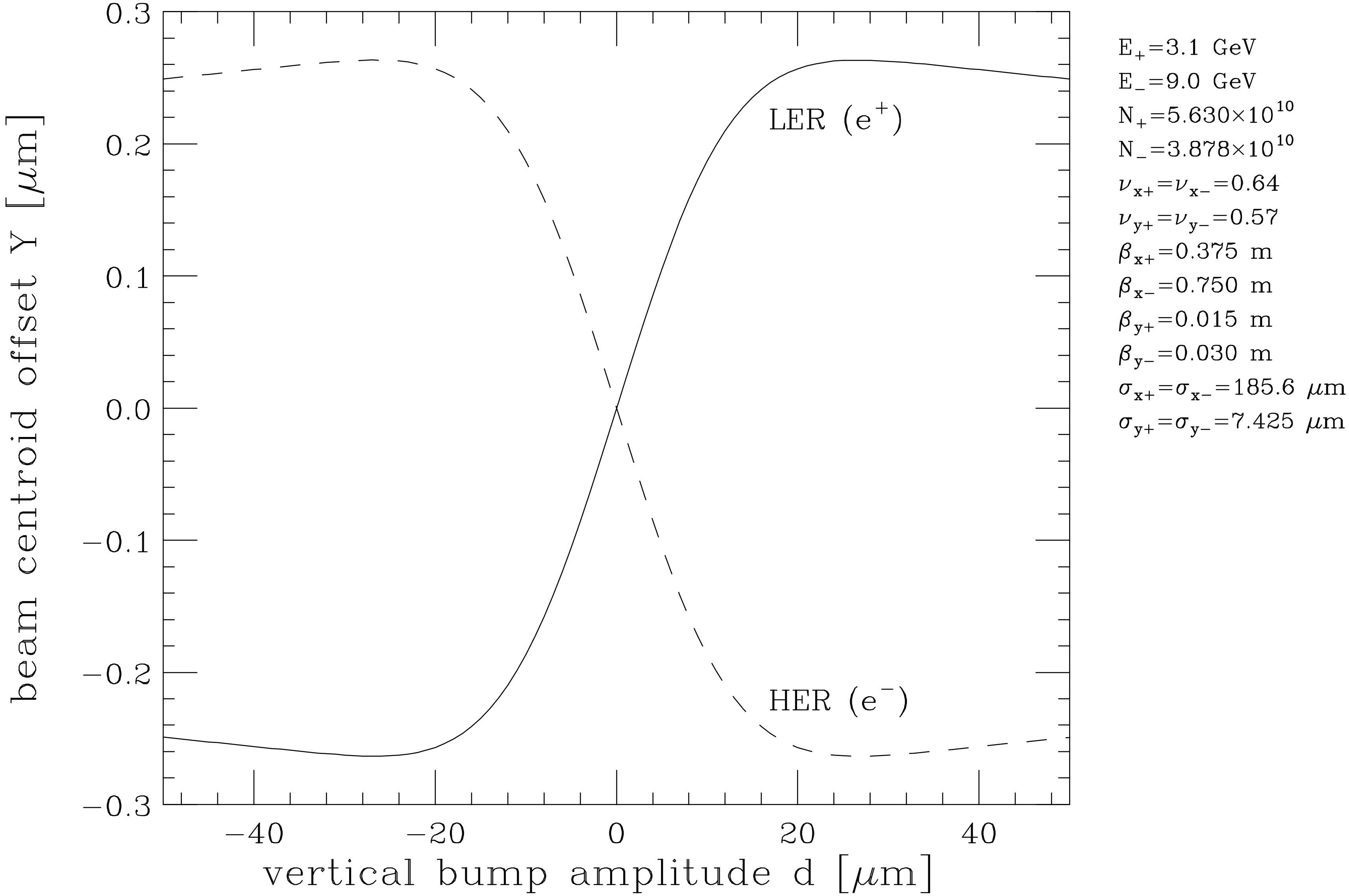

Fig. 3a. Vertical closed orbit distortions Y for both beams, plotted vs. the nominal vertical bump amplitude d (solid=LER, dashed=HER). Note that the distortions are of equal magnitude and opposite sign, as a consequence of the transparency symmetry, Eq. (2.35).

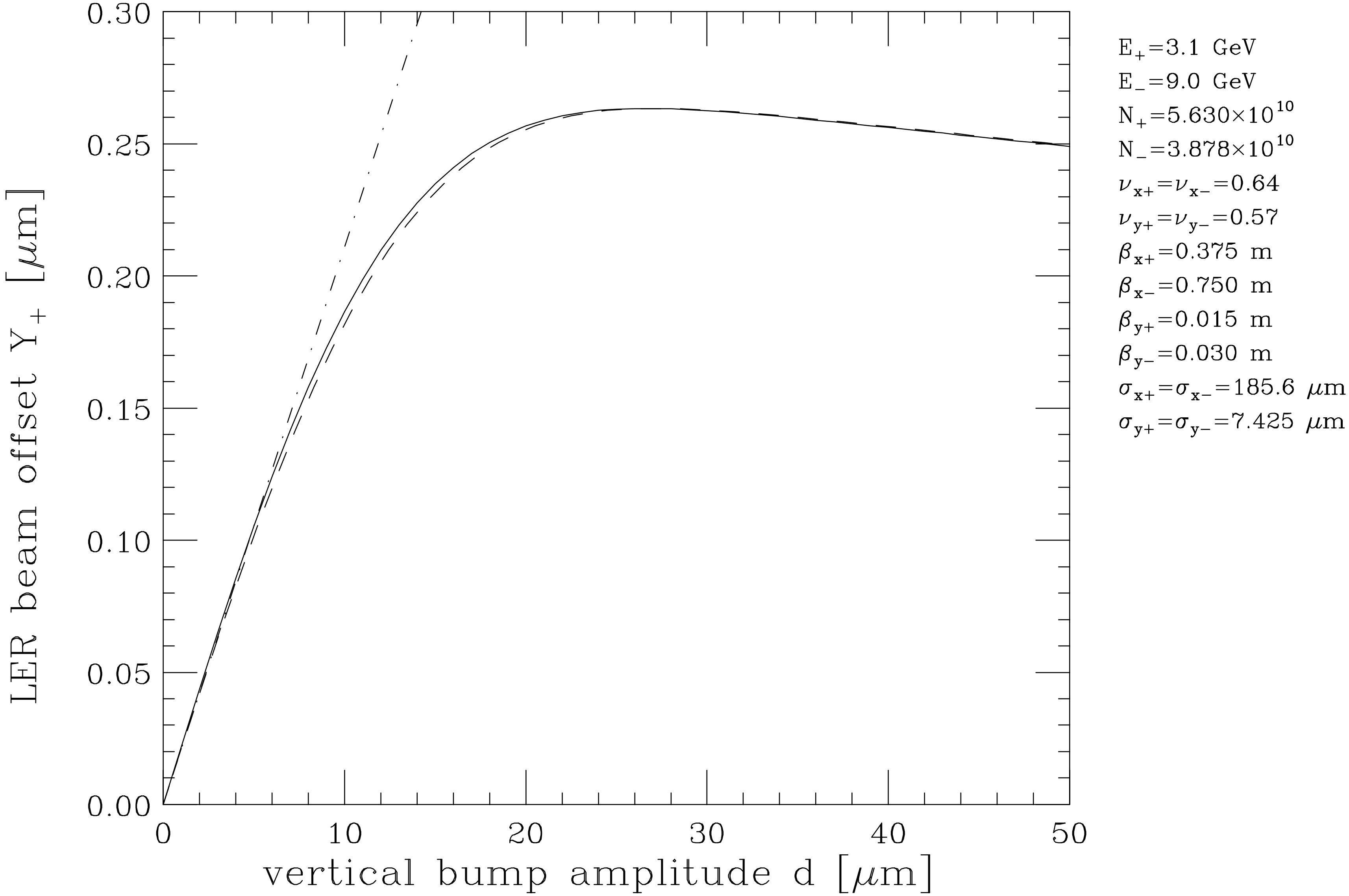

Fig. 3b. Magnified view of the LER's orbit offset. The solid line is the same as in Fig. 3a. The dot–dash line is the lowest–order approximation, Eq. (2.17). The dashed line shows the orbit offset plotted vs. the true separation between the orbits, $d+Y_+-Y_-$, rather than d.

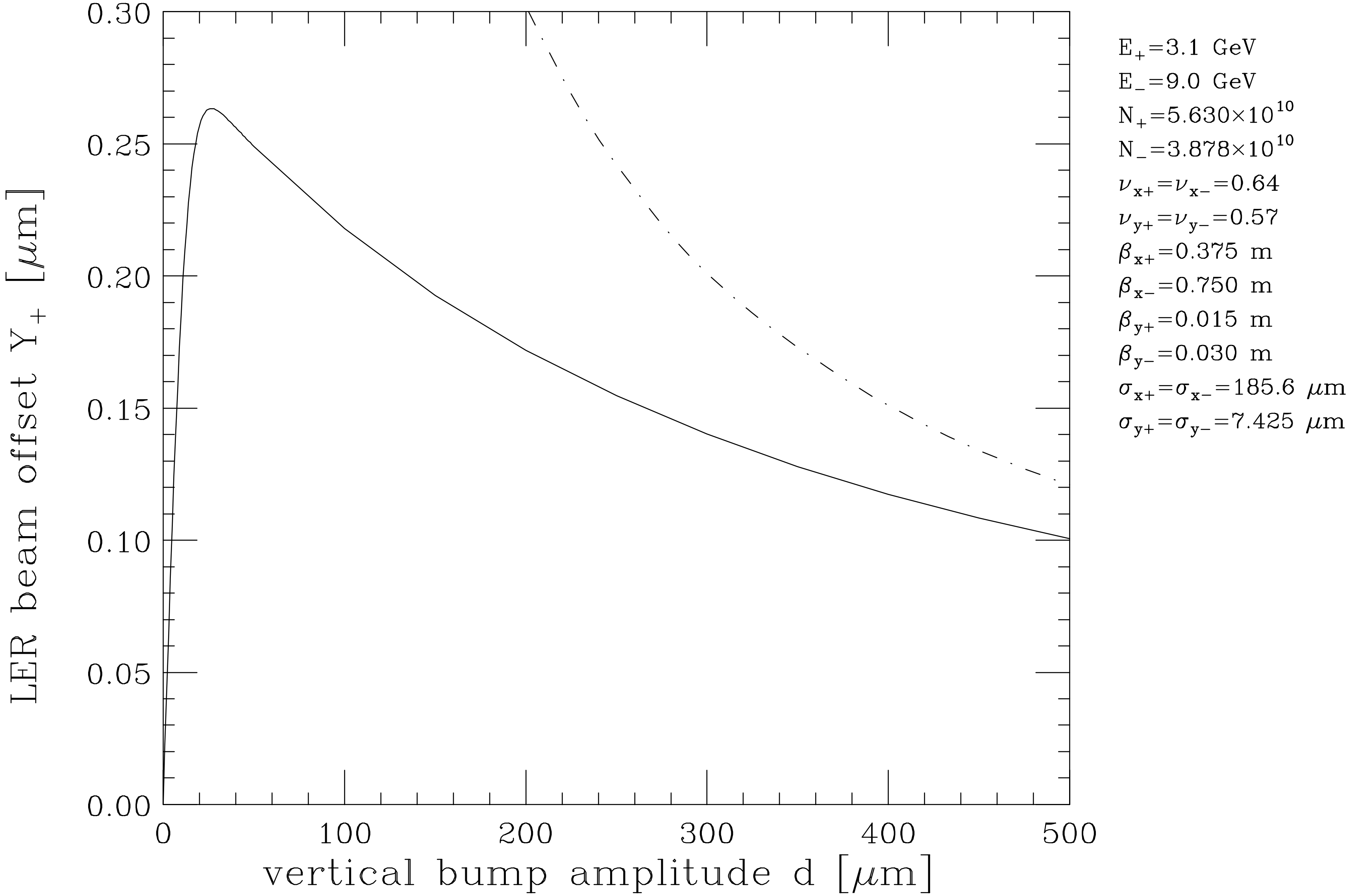

Fig. 3c. LER orbit offset for large values of the bump amplitude. The solid line is the same as in Fig. 3a. The dot–dash line is the asymptotic expression at large d, Eq. (2.19).

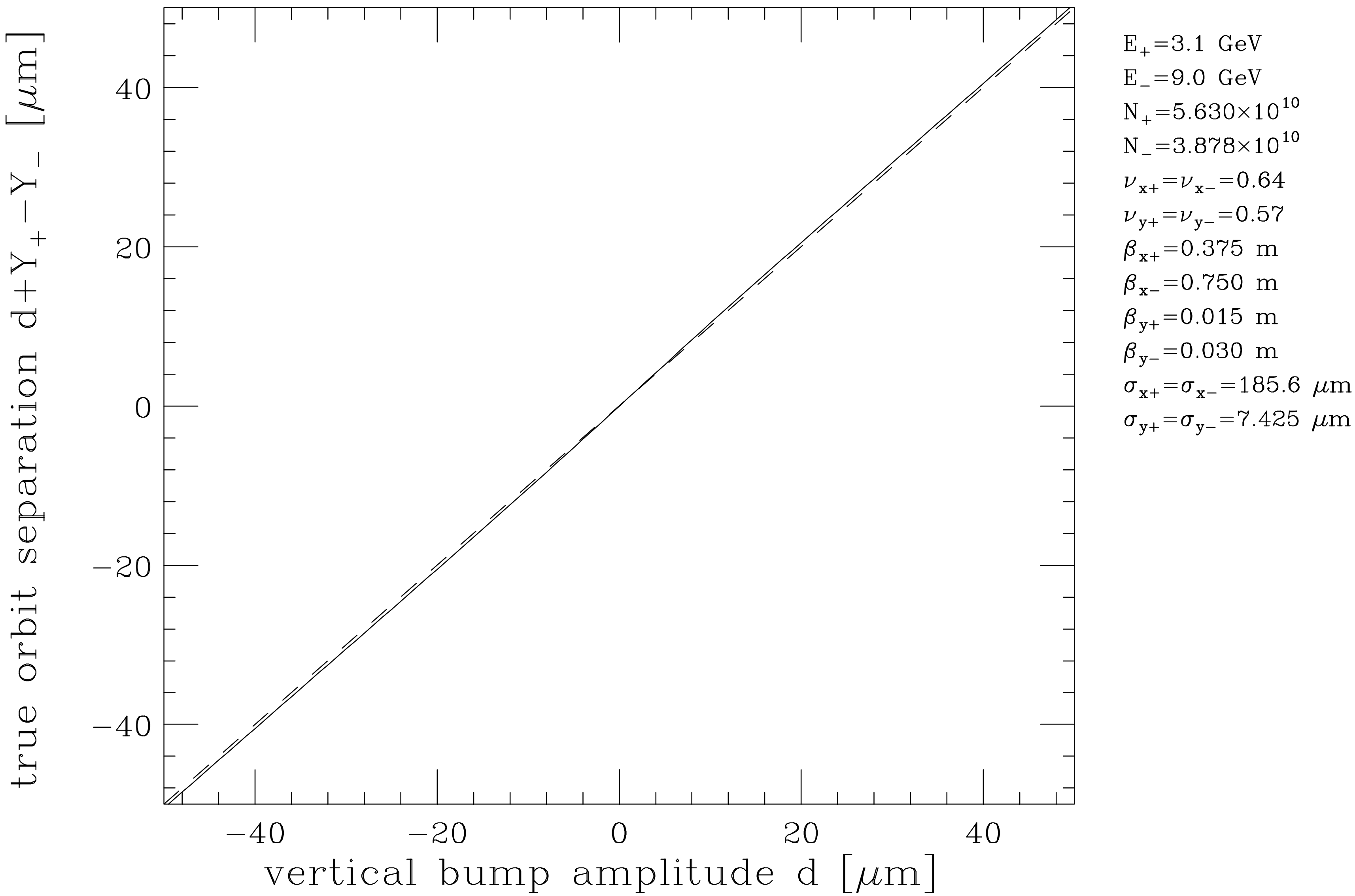

Fig. 4. True orbit separation at the IP (solid line). The dashed line is a straight line along the diagonal, for reference. The fact that the true separation is so close to a straight line is a reflection of the smallnes of the orbit distortions. This smallness is, in turn, a consequence of the smallness of ξ_0 and the closeness of ν_y to the half−integer.

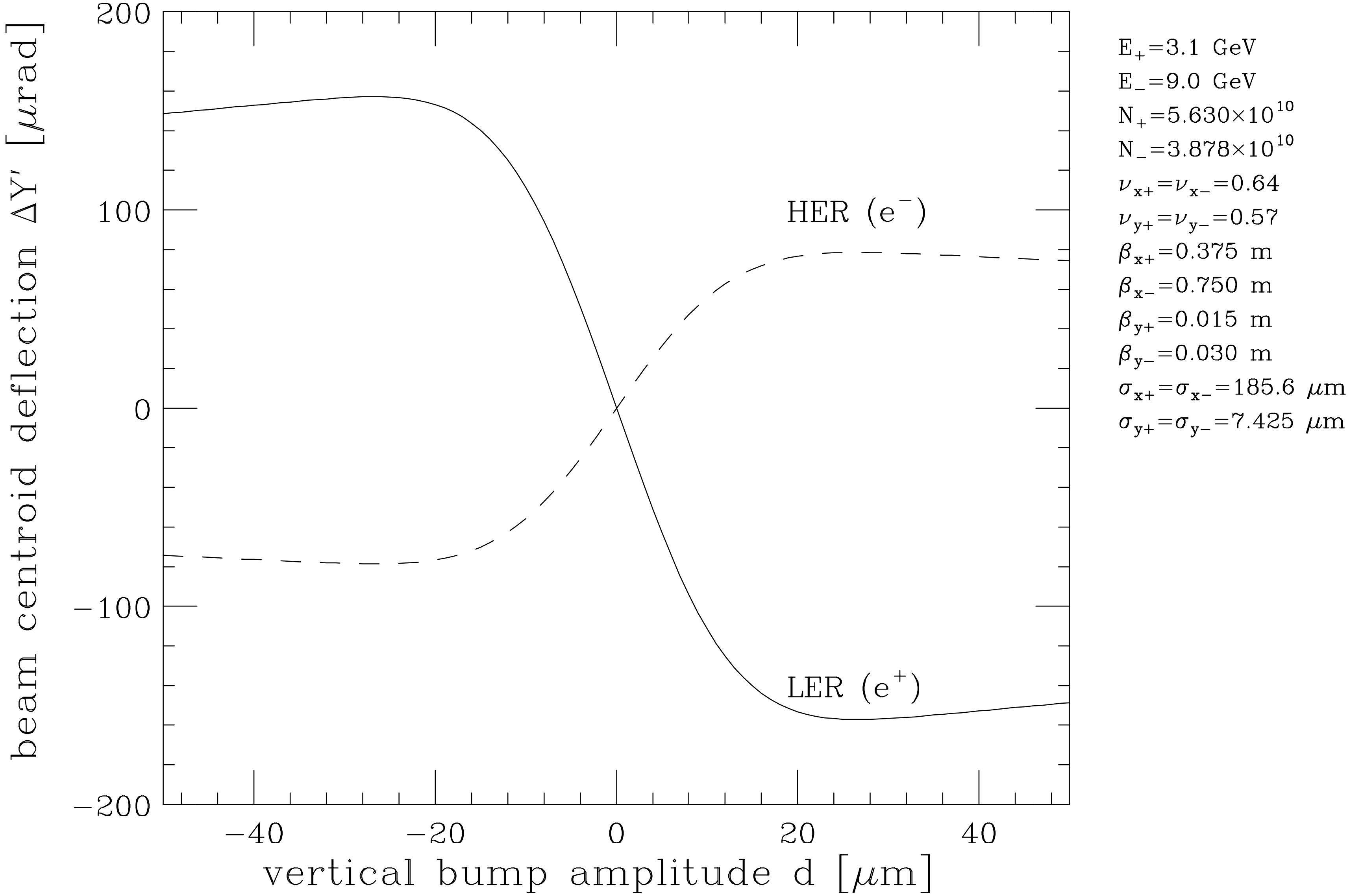

Fig. 5. Angular deflection of the beam centroids at the IP as a result of the beam−beam kick (solid=LER, dashed=HER). Note that the deflections are of opposite sign, and the magnitudes are in the ratio 2:1, as a consequence of the transparency symmetry, Eq. (2.35).

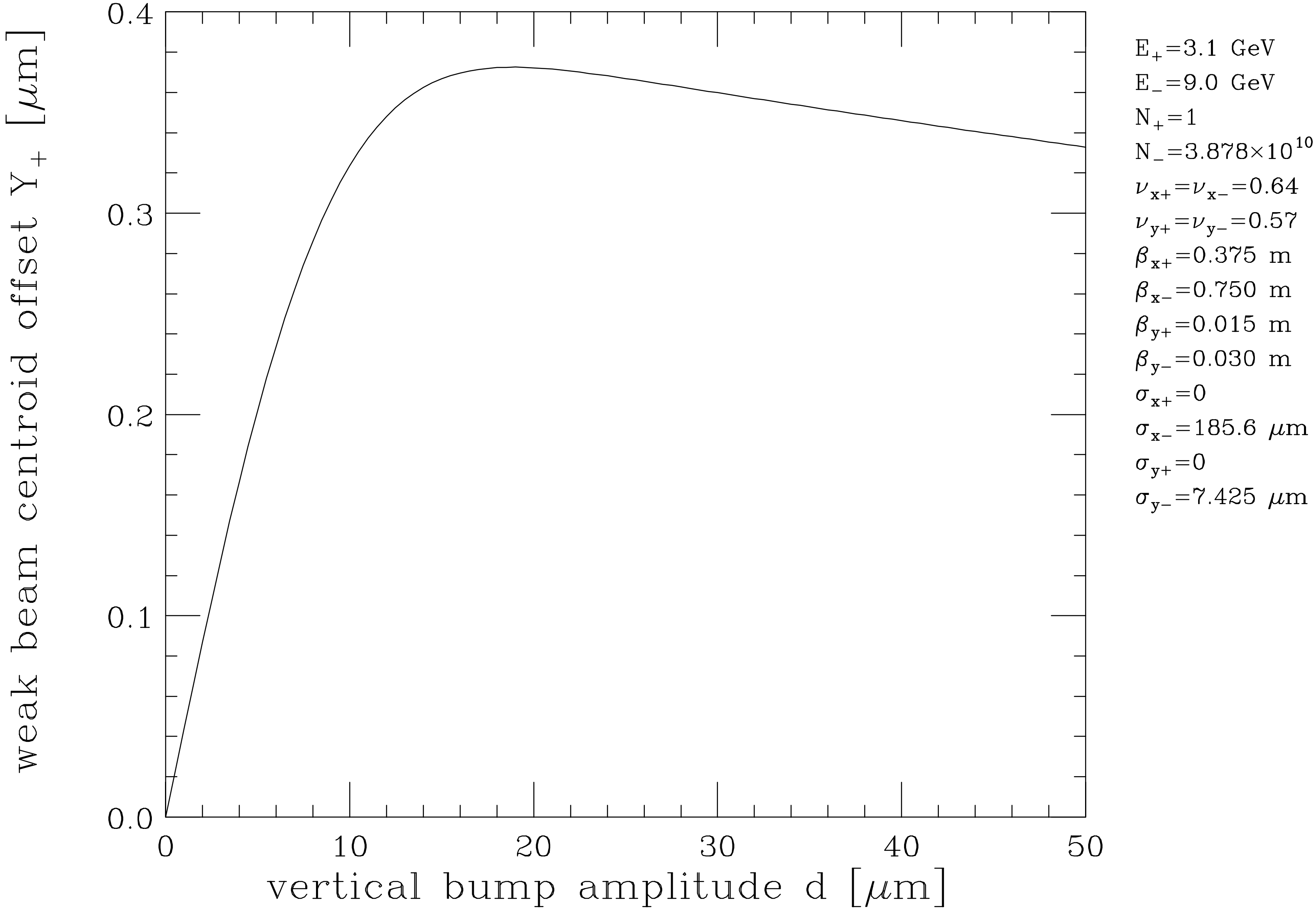

Fig. 6. Vertical closed orbit distortion at the IP of a weak beam consisting of a single positron. In this case the strong beam remains undisturbed.

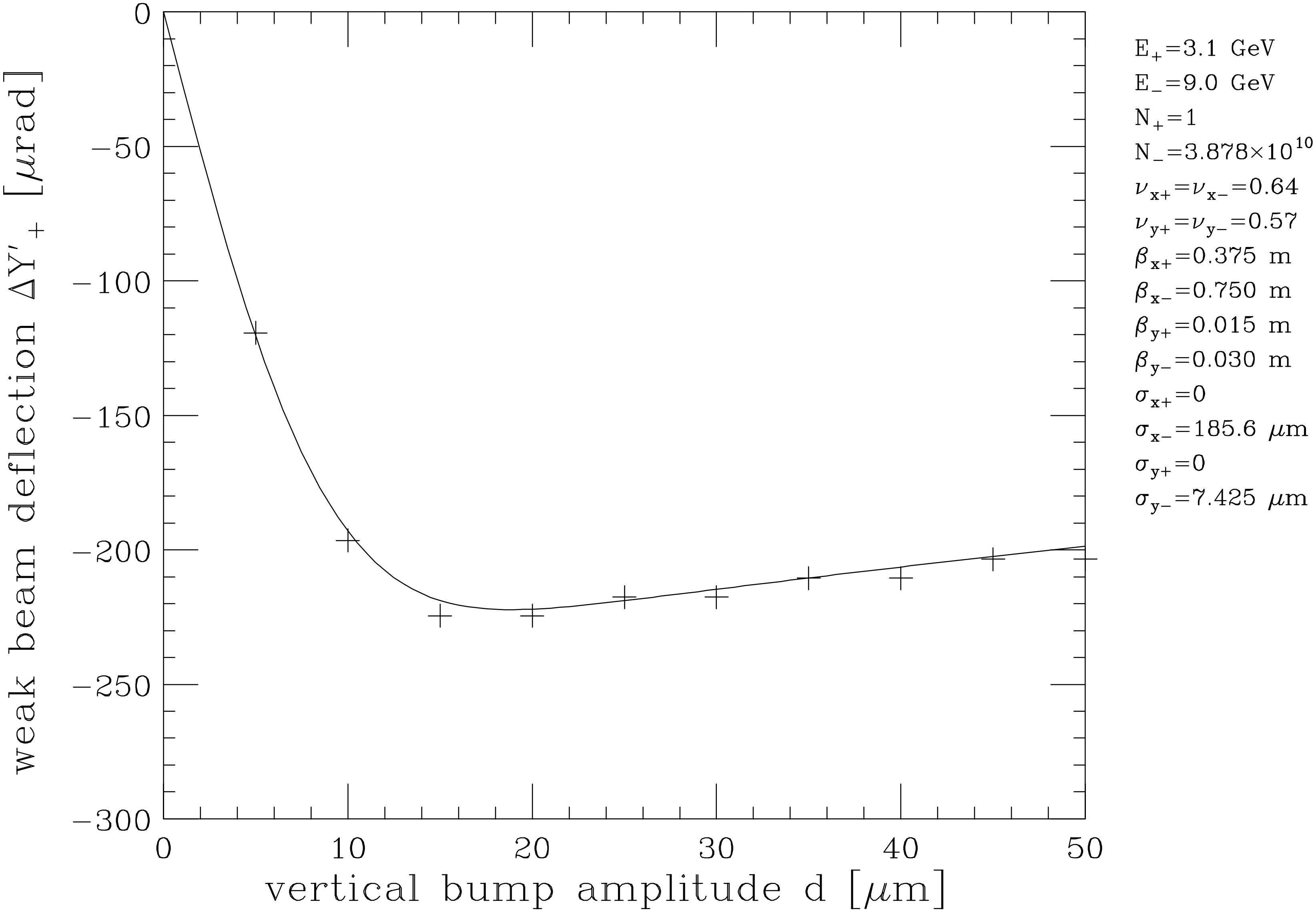

Fig. 7. Angular deflection at the IP of a weak beam consisting of a single positron. The "data points" were obtained by tracking a positron for a few hundred turns with Tennyson's code and then measuring Y′ from the resultant phase space plot.

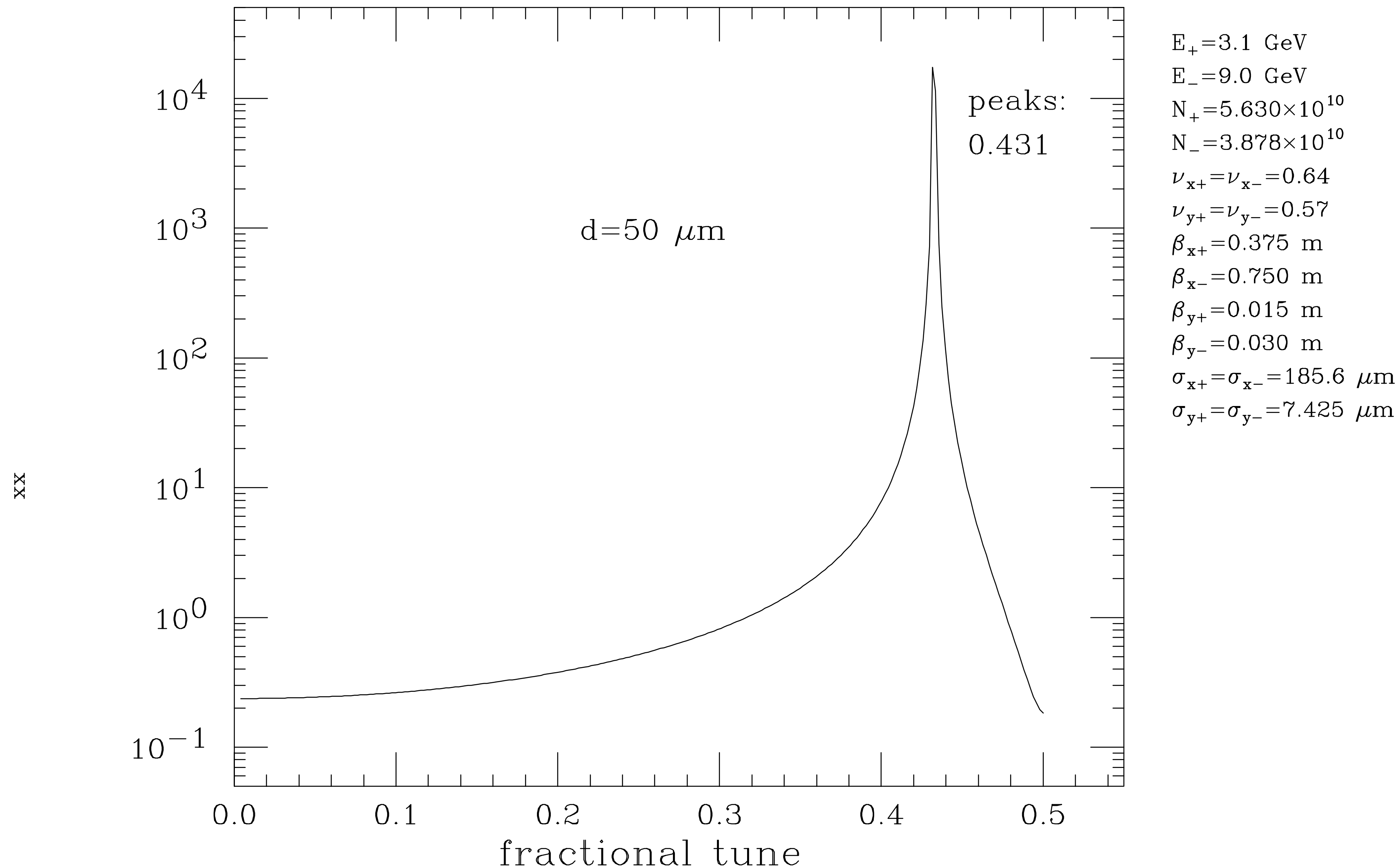

Fig. 8. Frequency spectrum of the vertical motion of the electron bunch centroid, for small−amplitude oscillations about the equilibrium closed orbit. The vertical bump amplitude is $d=50\mu m$. For this relatively large value there is only one peak near the mirror value of the vertical tune, $1-0.57=0.43$.

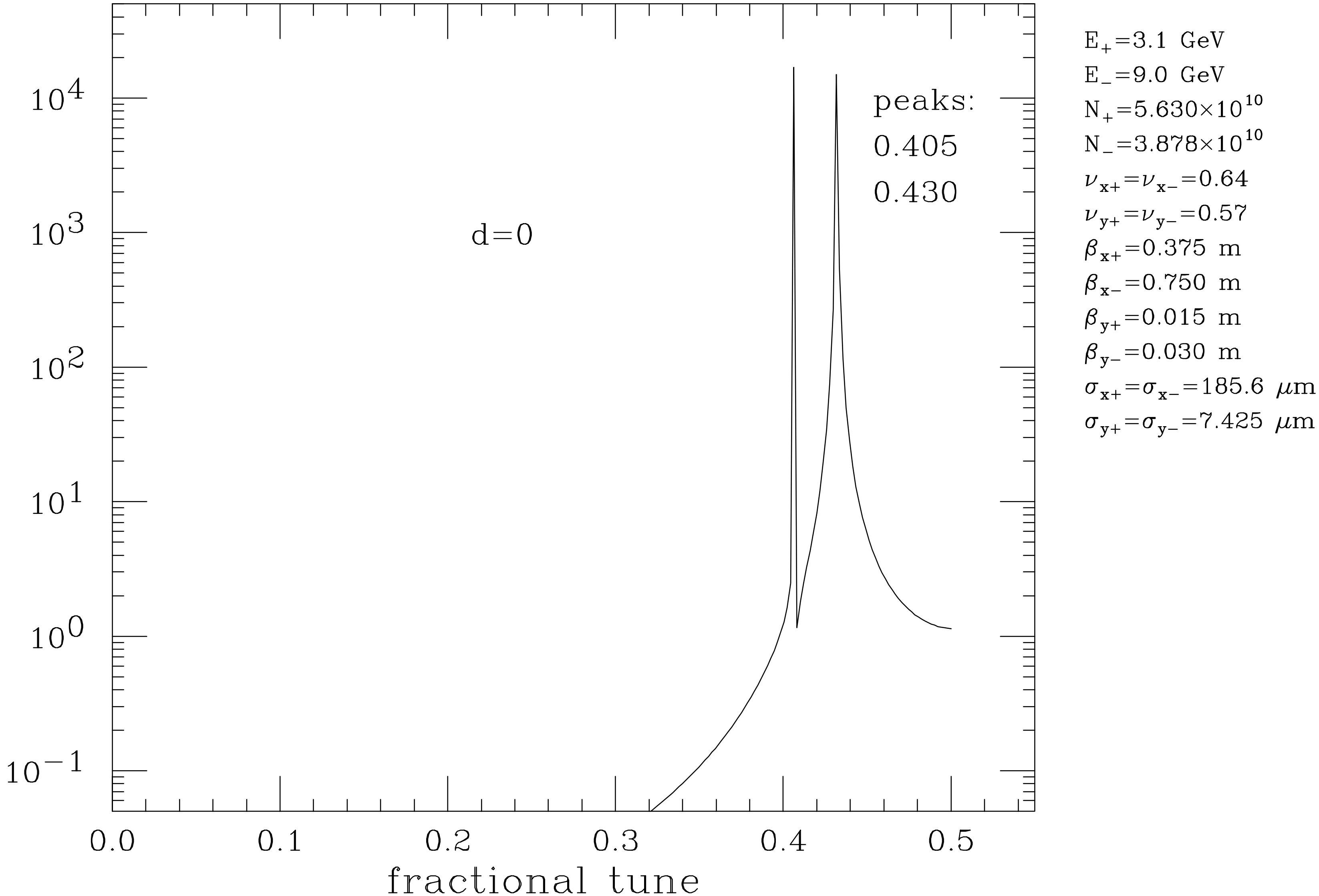

Fig. 9. Frequency spectrum of the vertical motion of the electron bunch centroid for small−amplitude oscillations about the equilibrium closed orbit, for head−on collisions. The peaks at 0.430 and 0.405 correspond to the σ and π modes, respectively. The tune split of 0.025 agrees very well with the analytical result obtained from Eq. (3.1).

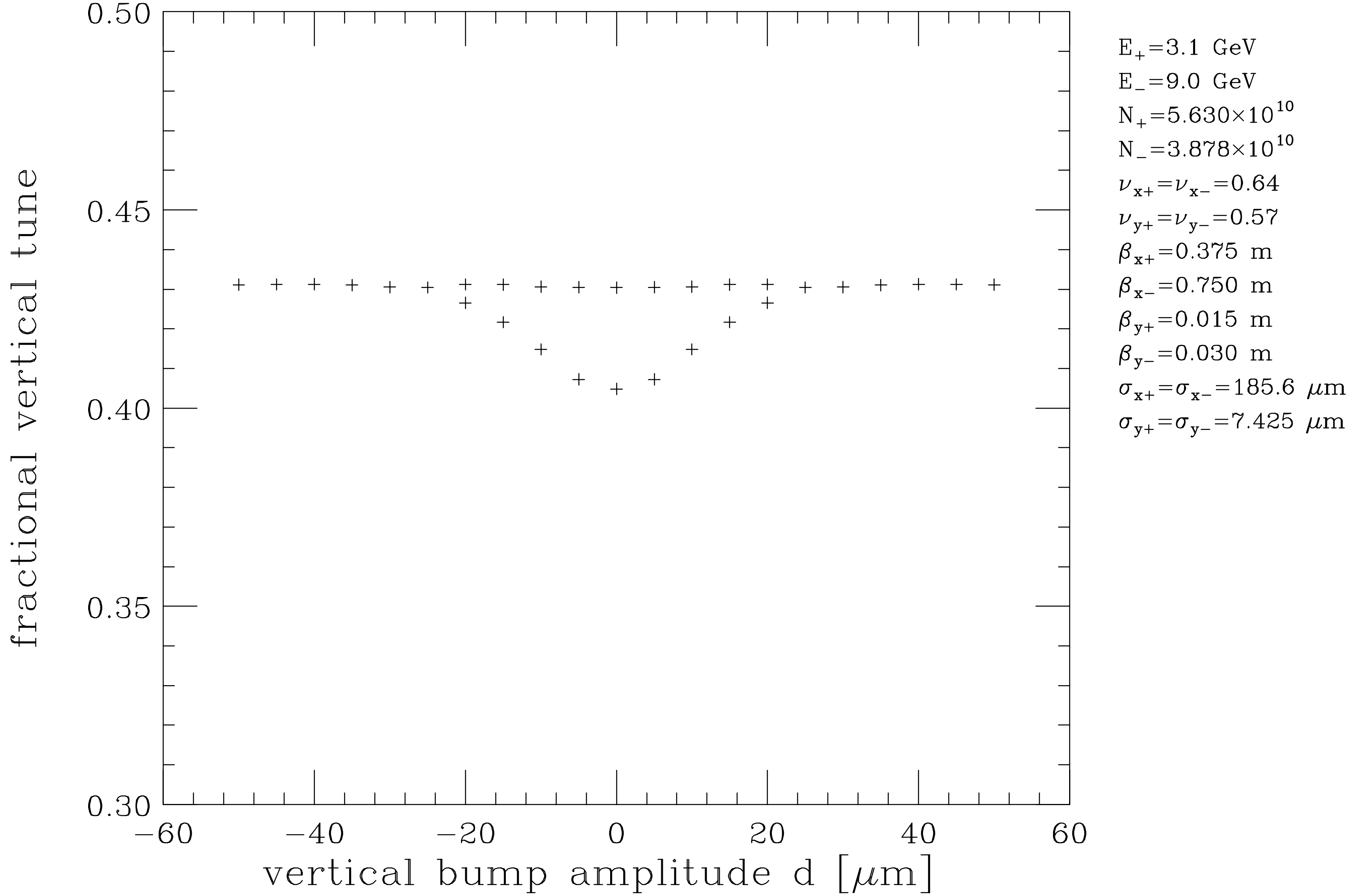

Fig. 10. Position of the σ and π peaks in the frequency spectrum of the vertical motion of the electron bunch centroid, as a function of vertical bump amplitude.

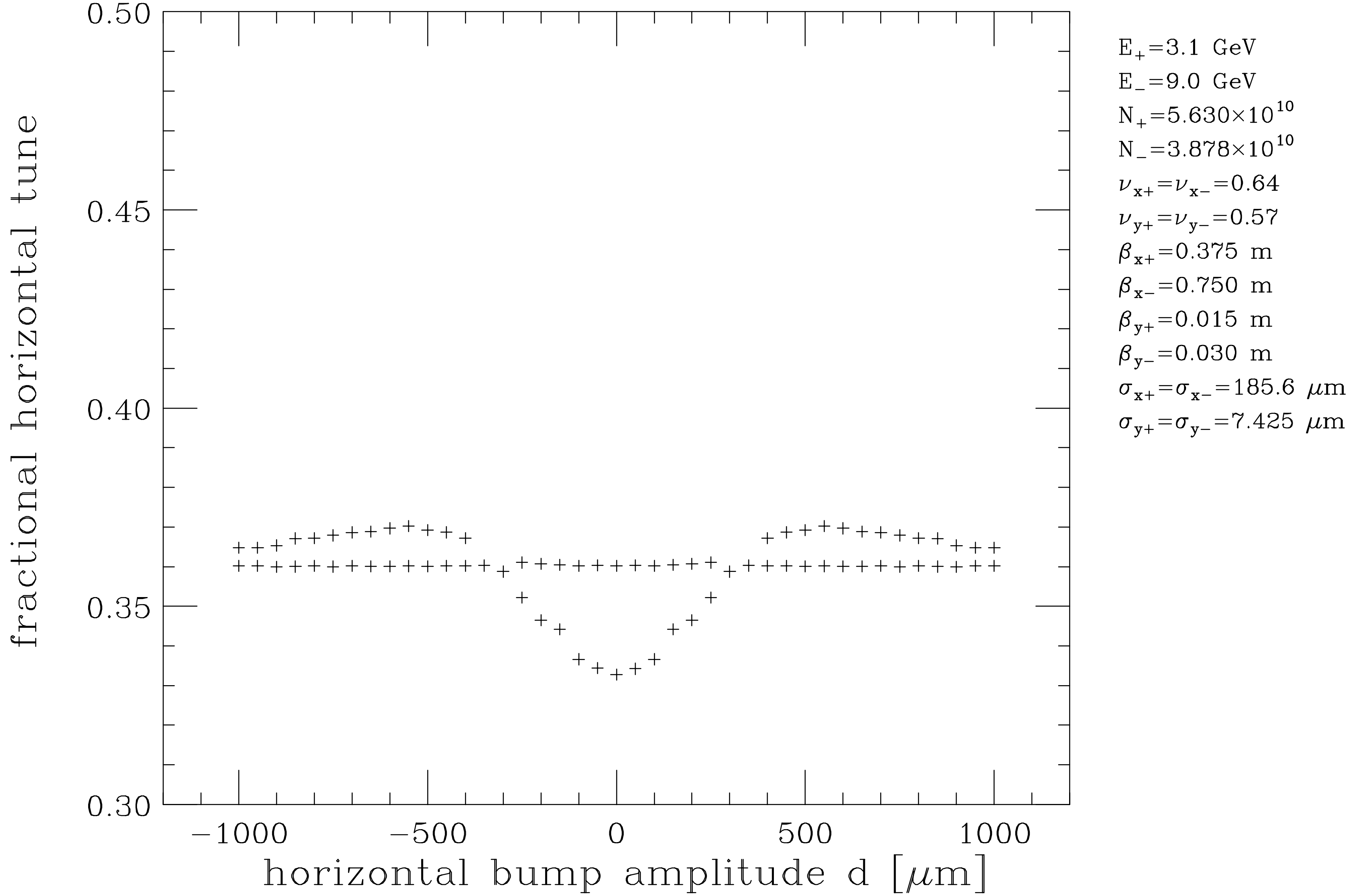

Fig. 11. Position of the σ and π peaks in the frequency spectrum of the horizontal motion of the electron bunch centroid, as a function of horizontal bump amplitude. In this case the vertical amplitude has been set to 0.

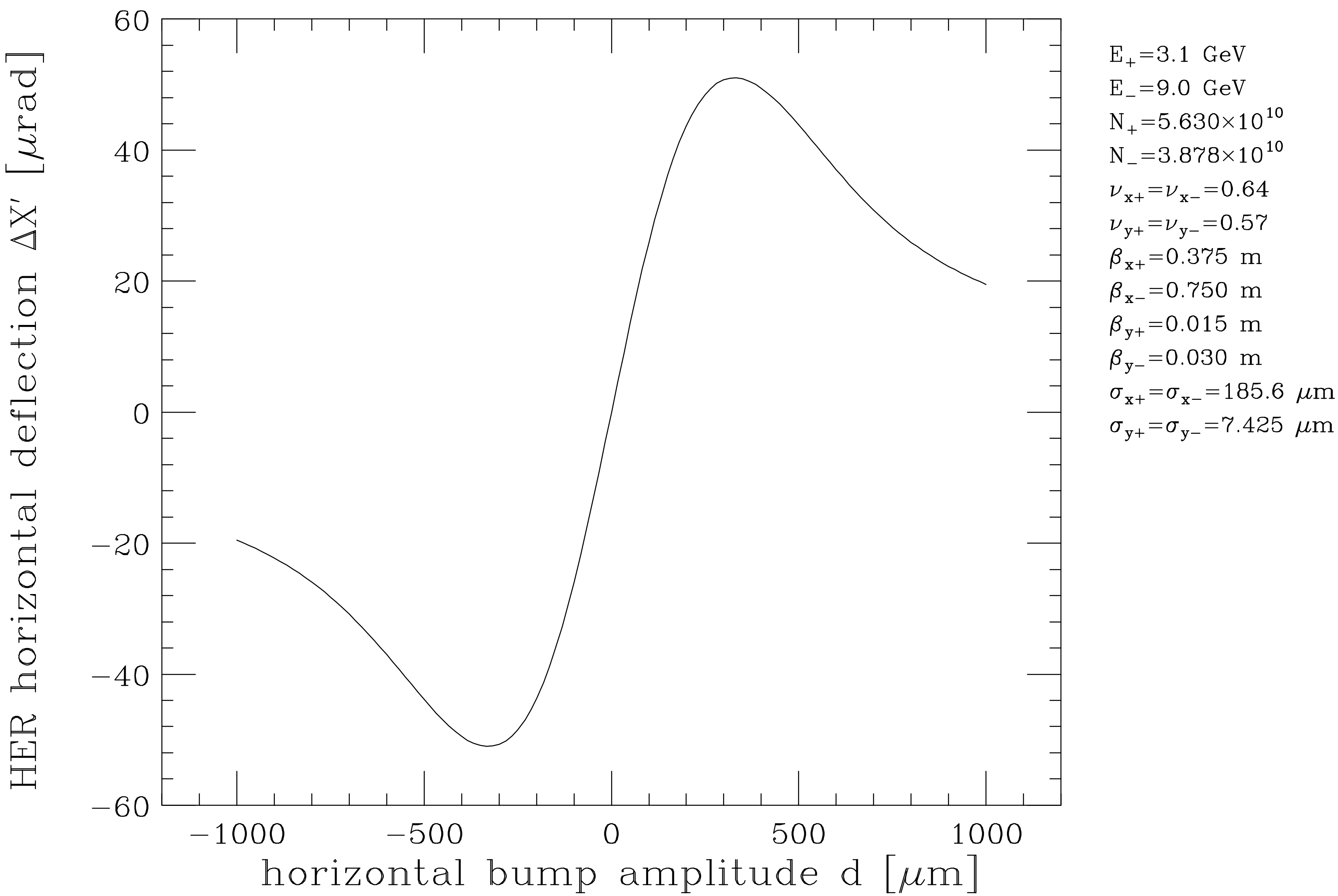

Fig. 12. Angular deflection at the IP of the electron beam centroid as a result of a beam−beam kick for horizontal, rather than vertical, bump amplitudes. Note that the curve falls off more quickly than in the vertical case, Fig. 5. The reason is that, for flat beams ($\sigma_y << \sigma_x$), the scale for the falloff of the beam−beam force in any direction is set by σ_x, while the scale for the rise is set by σ_y in the vertical direction, and by σ_x in the horizontal direction.

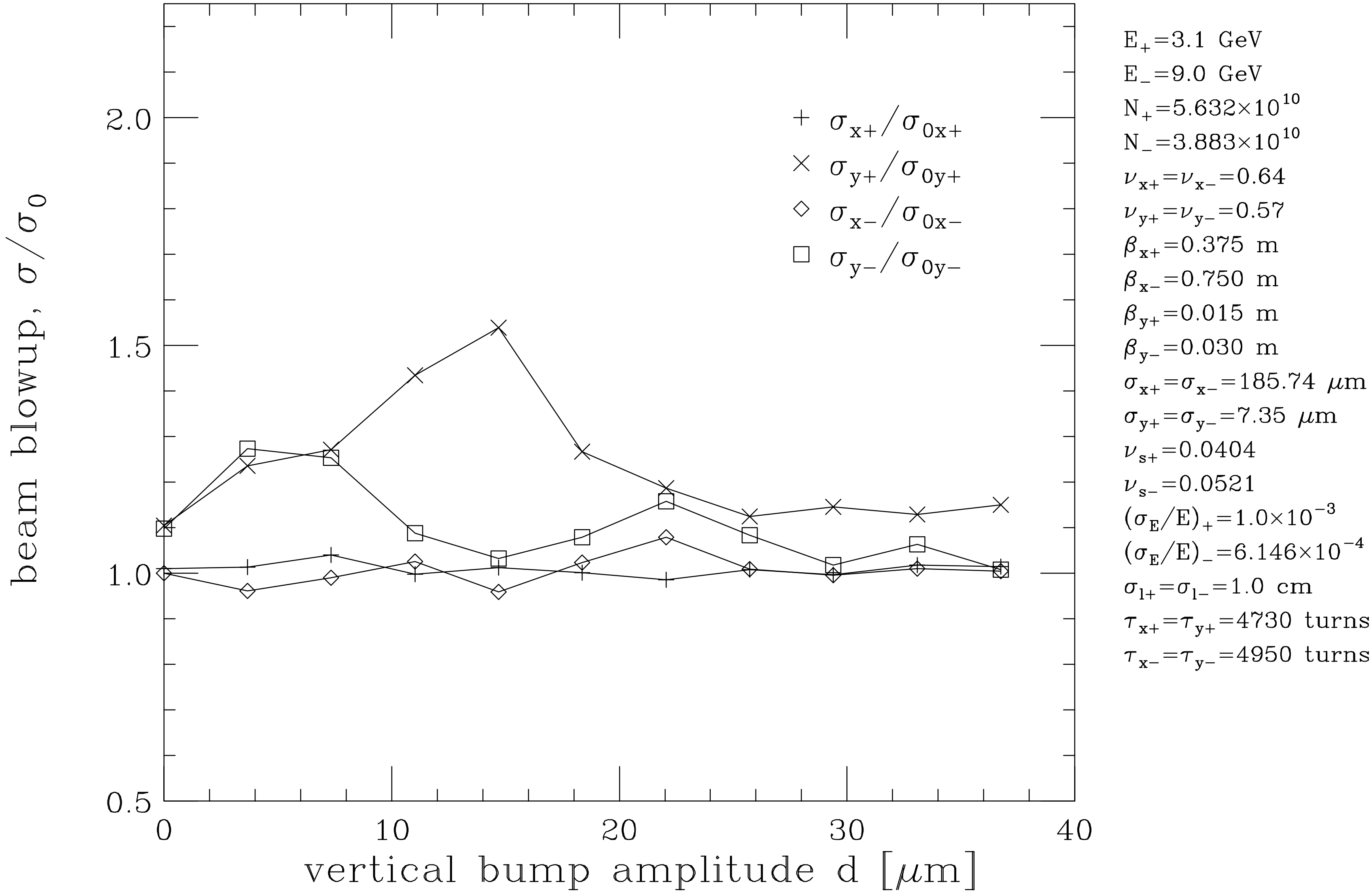

Fig. 13. Beam blowup relative to nominal beam size (Yokoya's code). Details of the simulation are explained in Sec. 4.

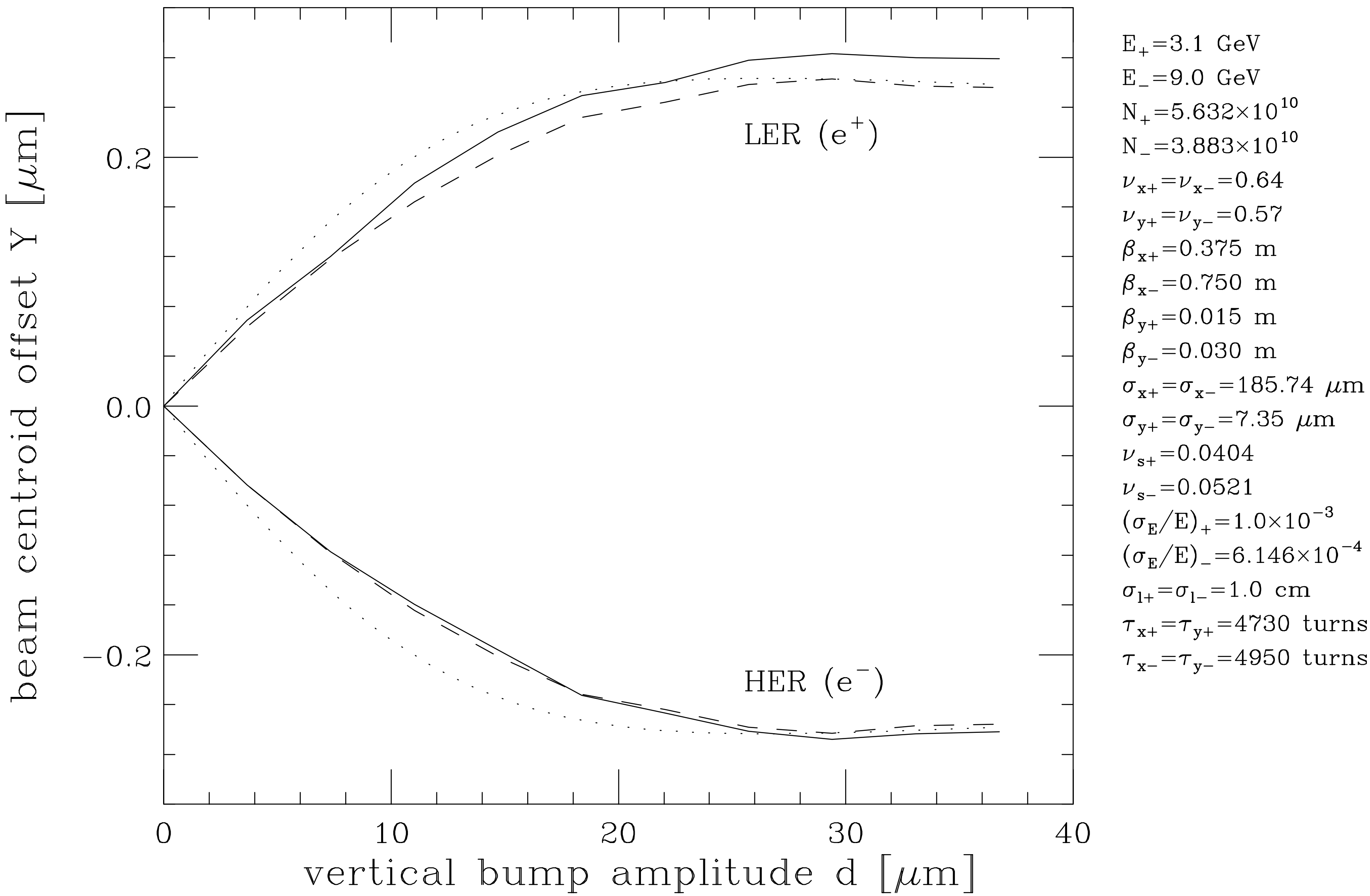

Fig. 14. Dependence of beam centroid offset on bump amplitude. The three sets of curves correspond to the full simulation using Yokoya's code (solid), the analytical result from Eq. (2.10) using nominal beam sizes (dotted), and the analytical result from Eq. (2.10) but using blown up beam sizes (dashed) as obtained from the full simulation and shown in Fig. 13.

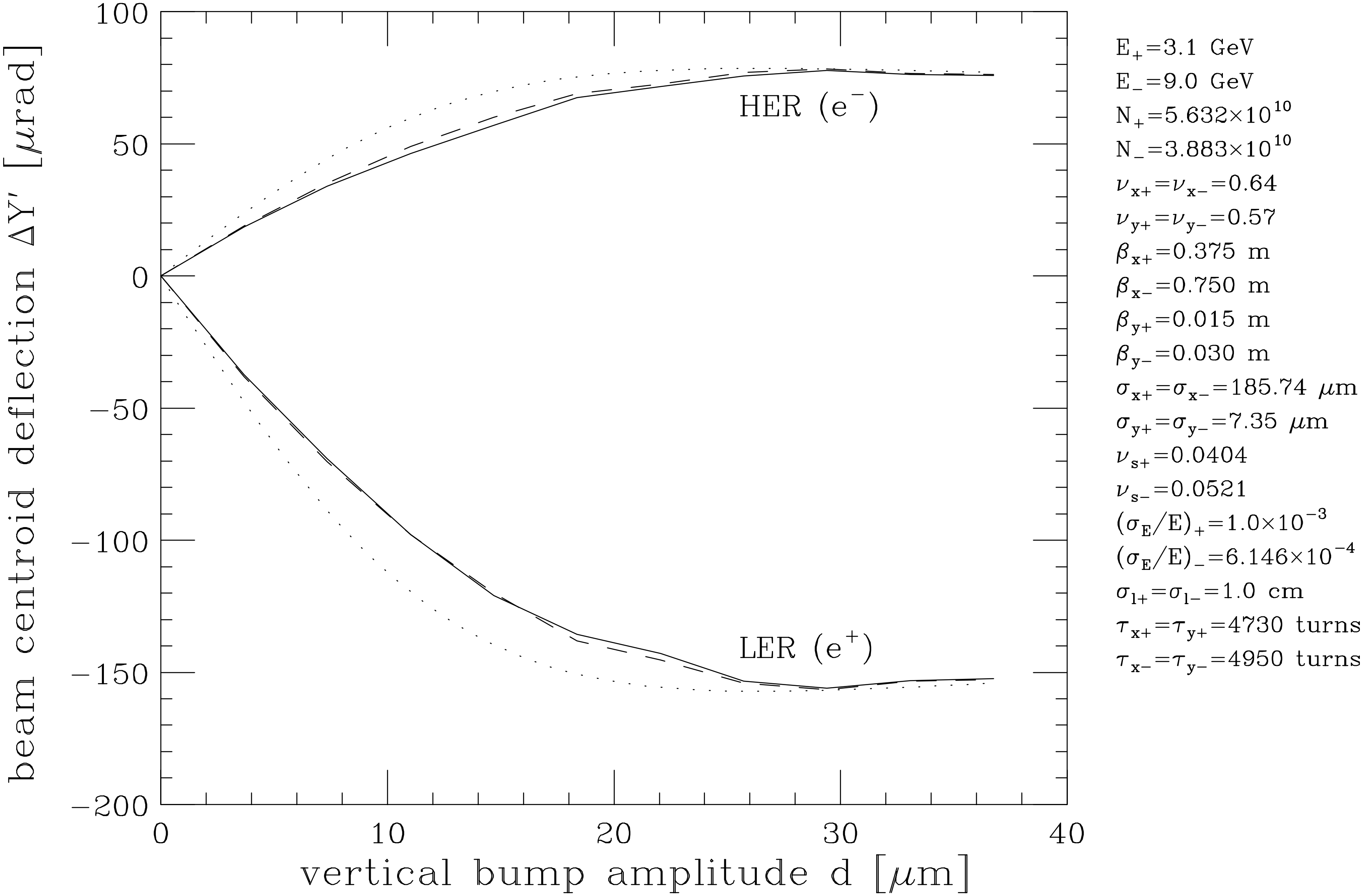

Fig. 15. Dependence of beam centroid deflection on bump amplitude. The three sets of

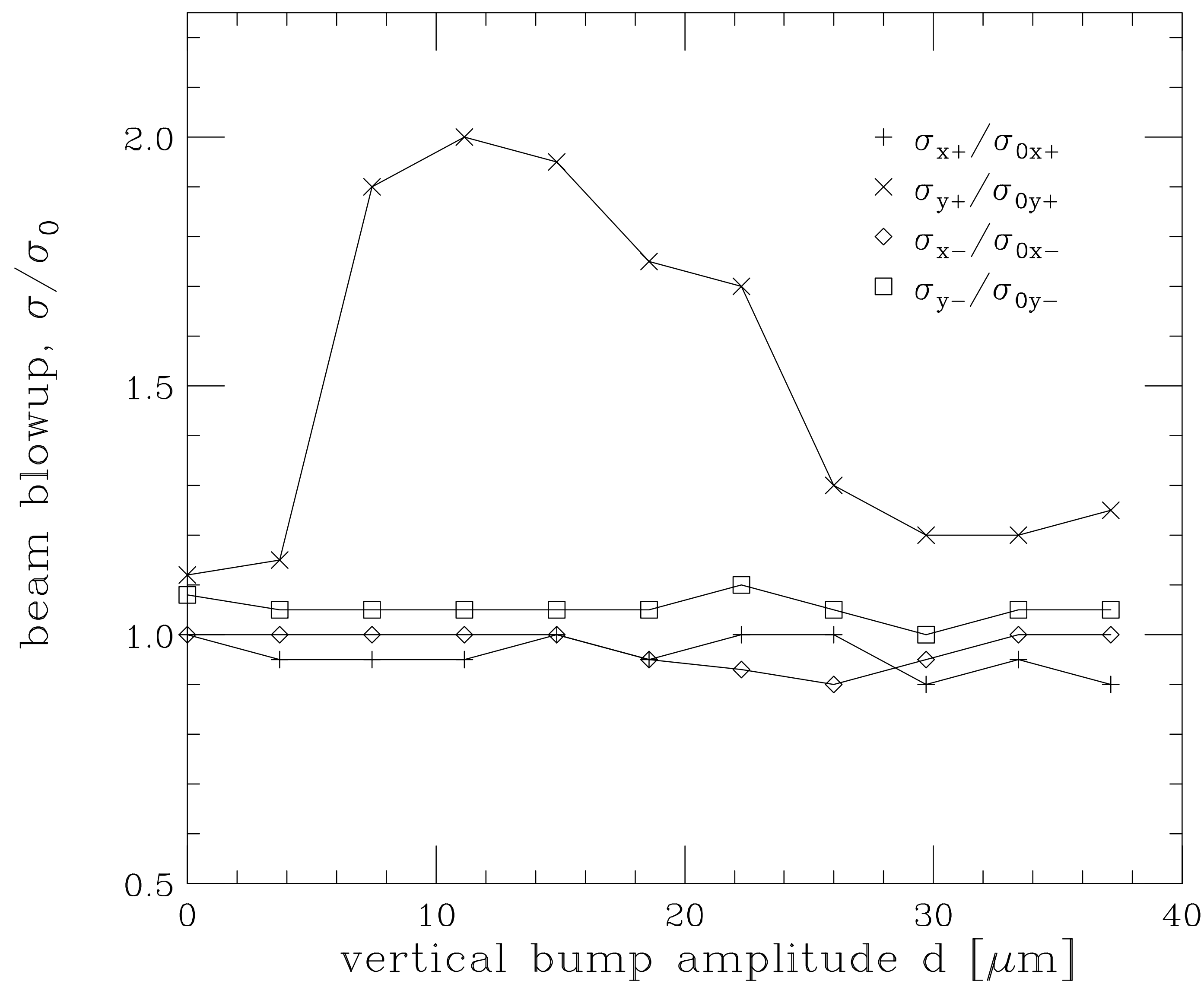

E_+=3.1 GeV
E_-=9.0 GeV
$N_+=5.7\times10^{10}$
$N_-=3.9\times10^{10}$
$\nu_{x+}=\nu_{x-}=0.64$
$\nu_{y+}=\nu_{y-}=0.57$
$\beta_{x+}=0.375$ m
$\beta_{x-}=0.750$ m
$\beta_{y+}=0.015$ m
$\beta_{y-}=0.030$ m
$\sigma_{x+}=\sigma_{x-}=186$ μm
$\sigma_{y+}=\sigma_{y-}=7.35$ μm
$\nu_{s+}=0.0403$
$\nu_{s-}=0.0519$
$(\sigma_E/E)_+=1.0\times10^{-3}$
$(\sigma_E/E)_-=6.1\times10^{-4}$
$\sigma_{l+}=\sigma_{l-}=1.0$ cm
$\tau_{x+,-}=\tau_{y+,-}=5014$ turns

Fig. 16. Beam blowup relative to nominal size (Tennyson's code).

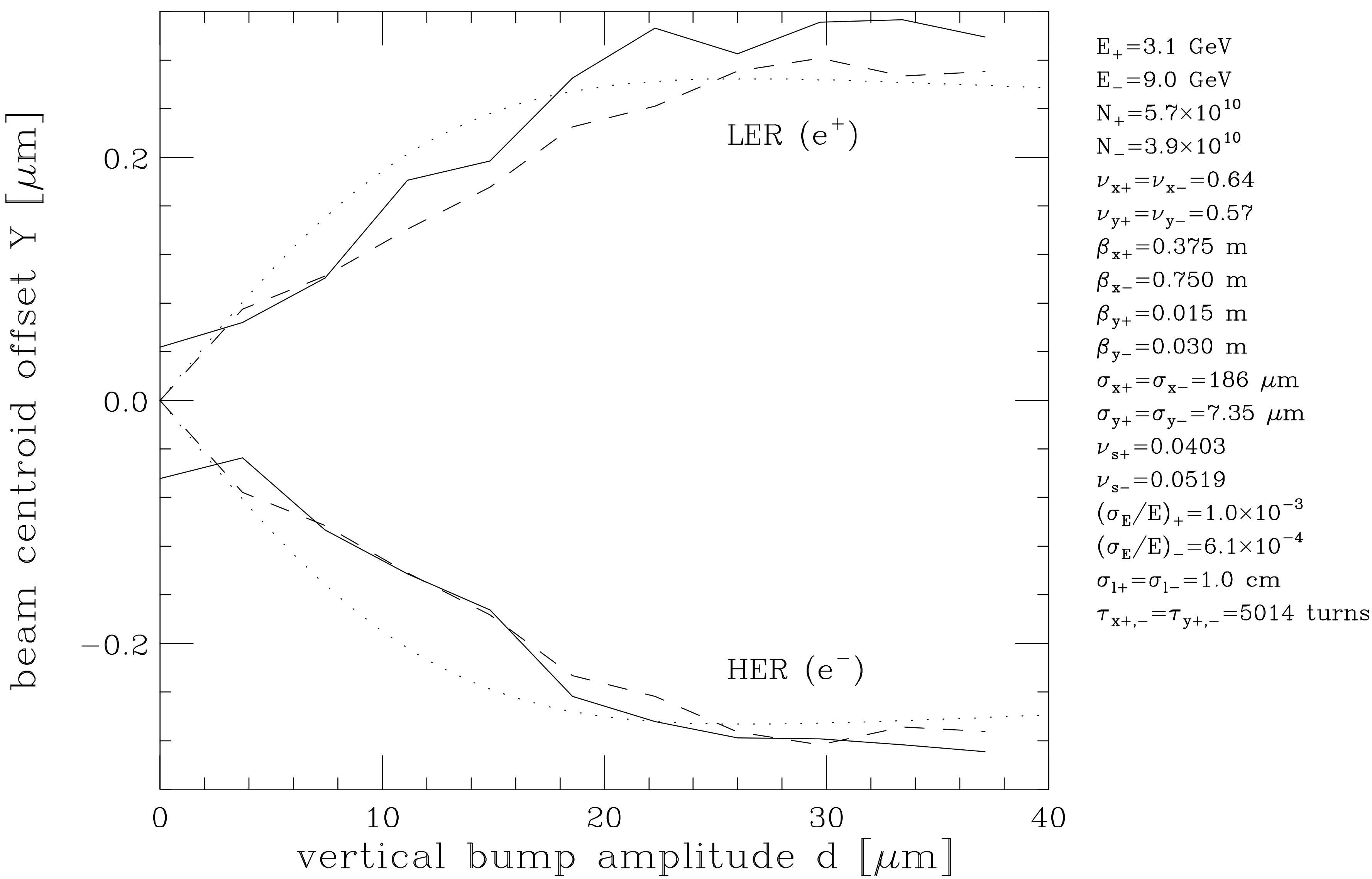

Fig. 17. Dependence of beam centroid offset on bump amplitude. The three sets of curves correspond to the full simulation using Tennyson's code (solid), the analytical result from Eq. (2.10) using nominal beam sizes (dotted), and the analytical result from Eq. (2.10) but using the blown up beam sizes (dashed) shown in Fig. 16. Fig. 16. The nonzero offset at d=0 is due to the statistical error affecting the centroid calculation, which uses a relatively coarse sampling; it is representative of the statistical fluctuations at all beam separations.

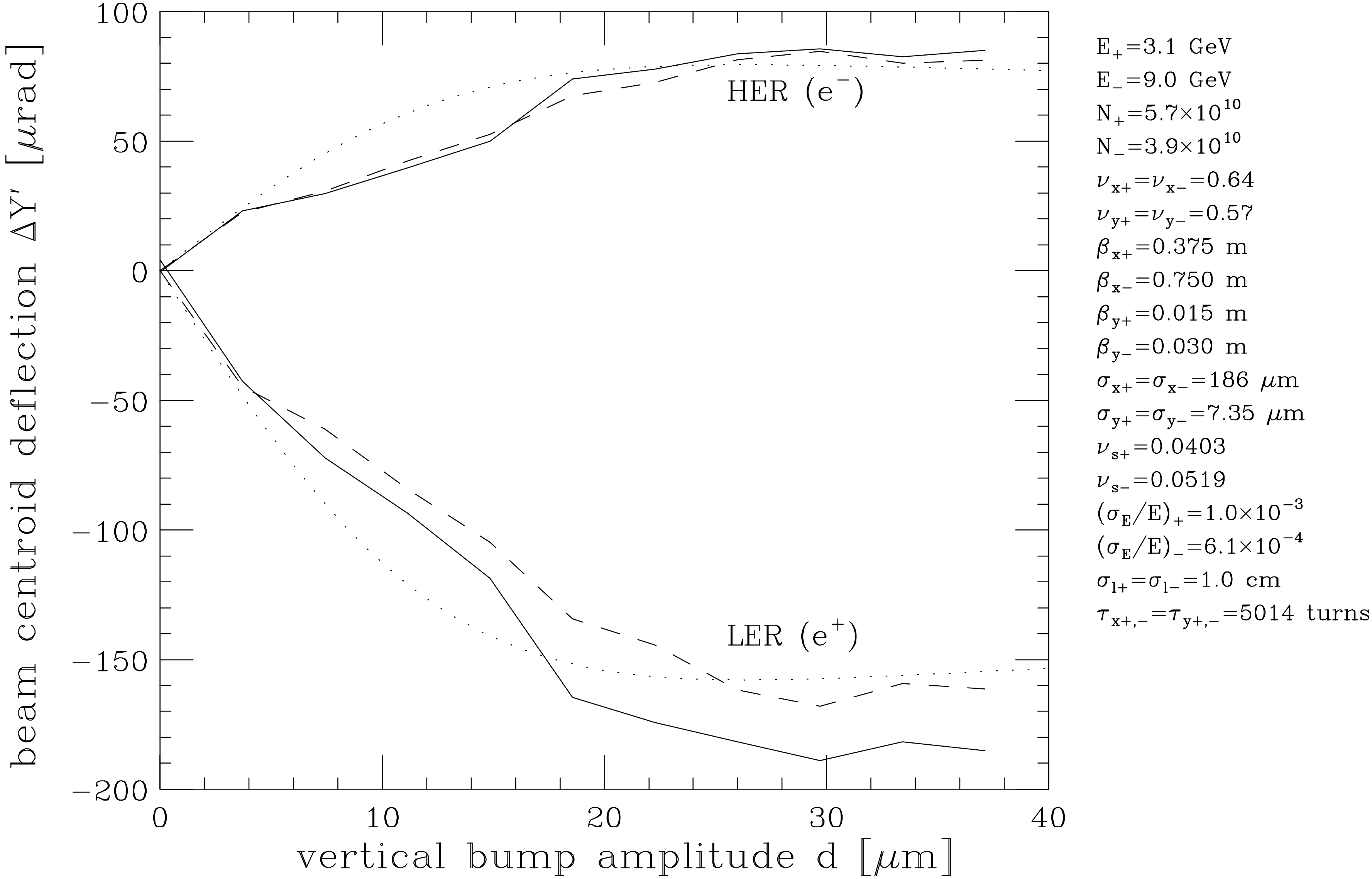

Fig. 18. Dependence of beam centroid deflection on bump amplitude. The three sets of curves parallel those in Fig. 17 (Tennyson's code).

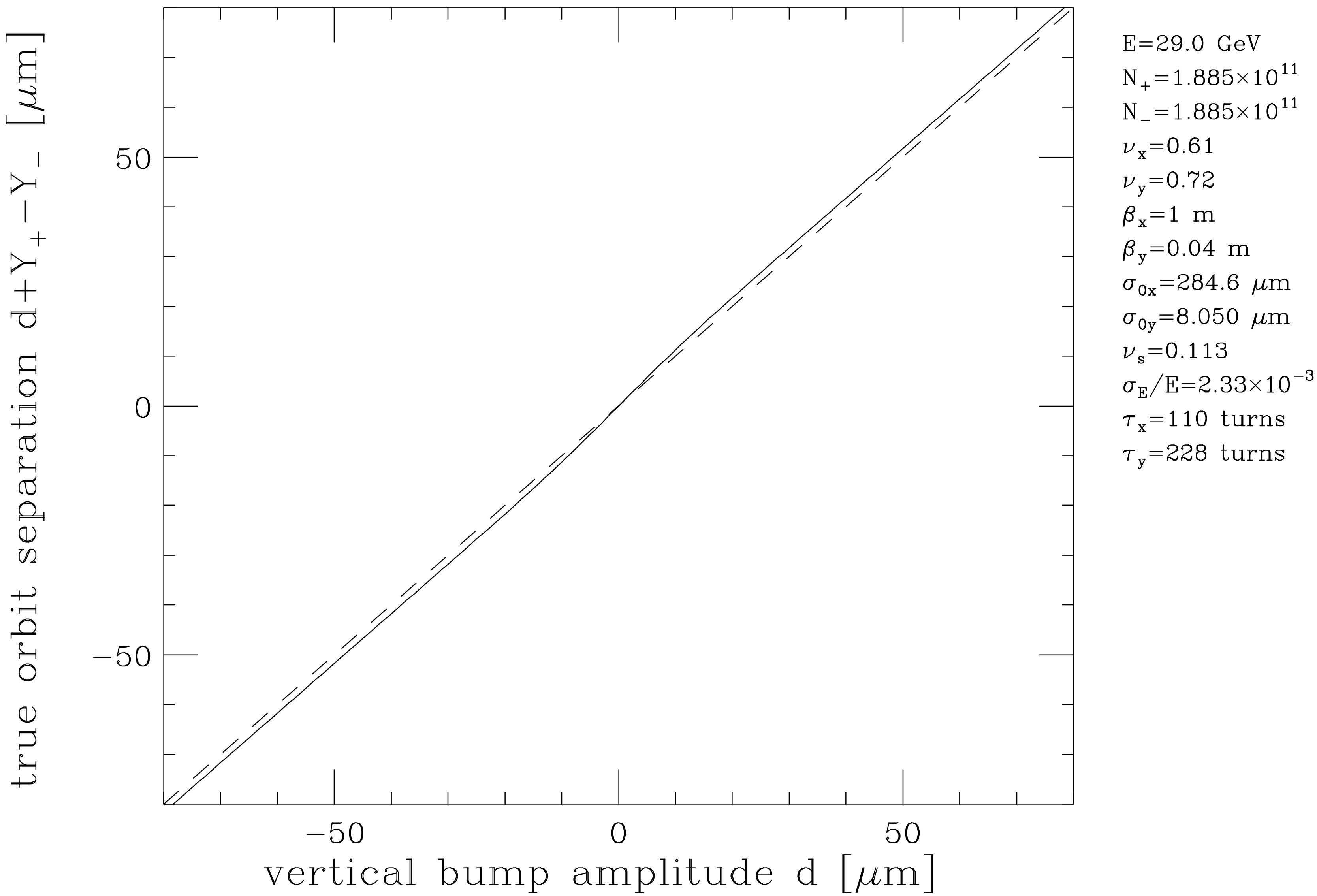

Fig. 19. True orbit separation at the IP (solid line) for TRISTAN. The dashed line is a straight line along the diagonal, for reference.

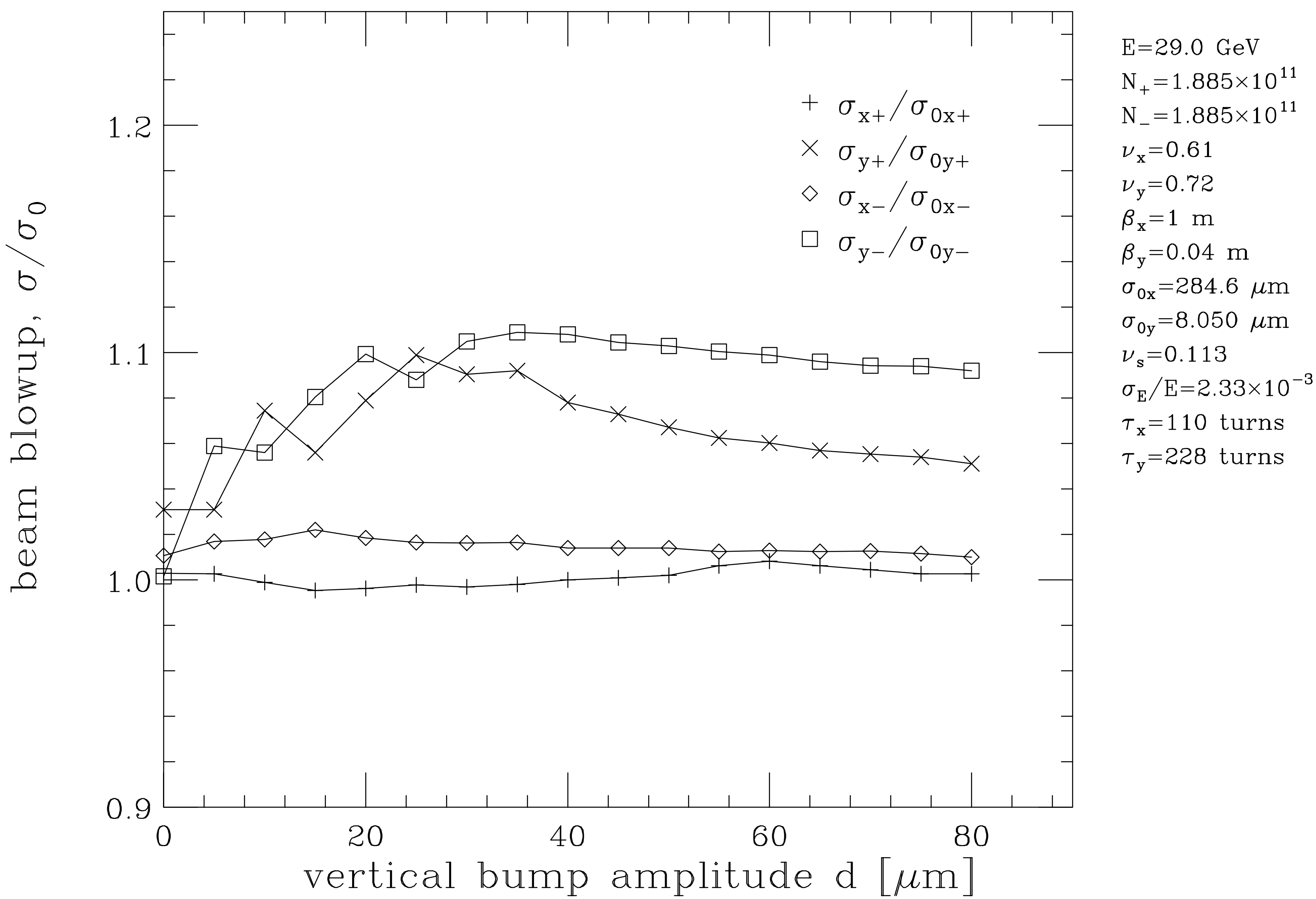

Fig. 20. Beam blowup relative to nominal beam size for TRISTAN (Yokoya's code).

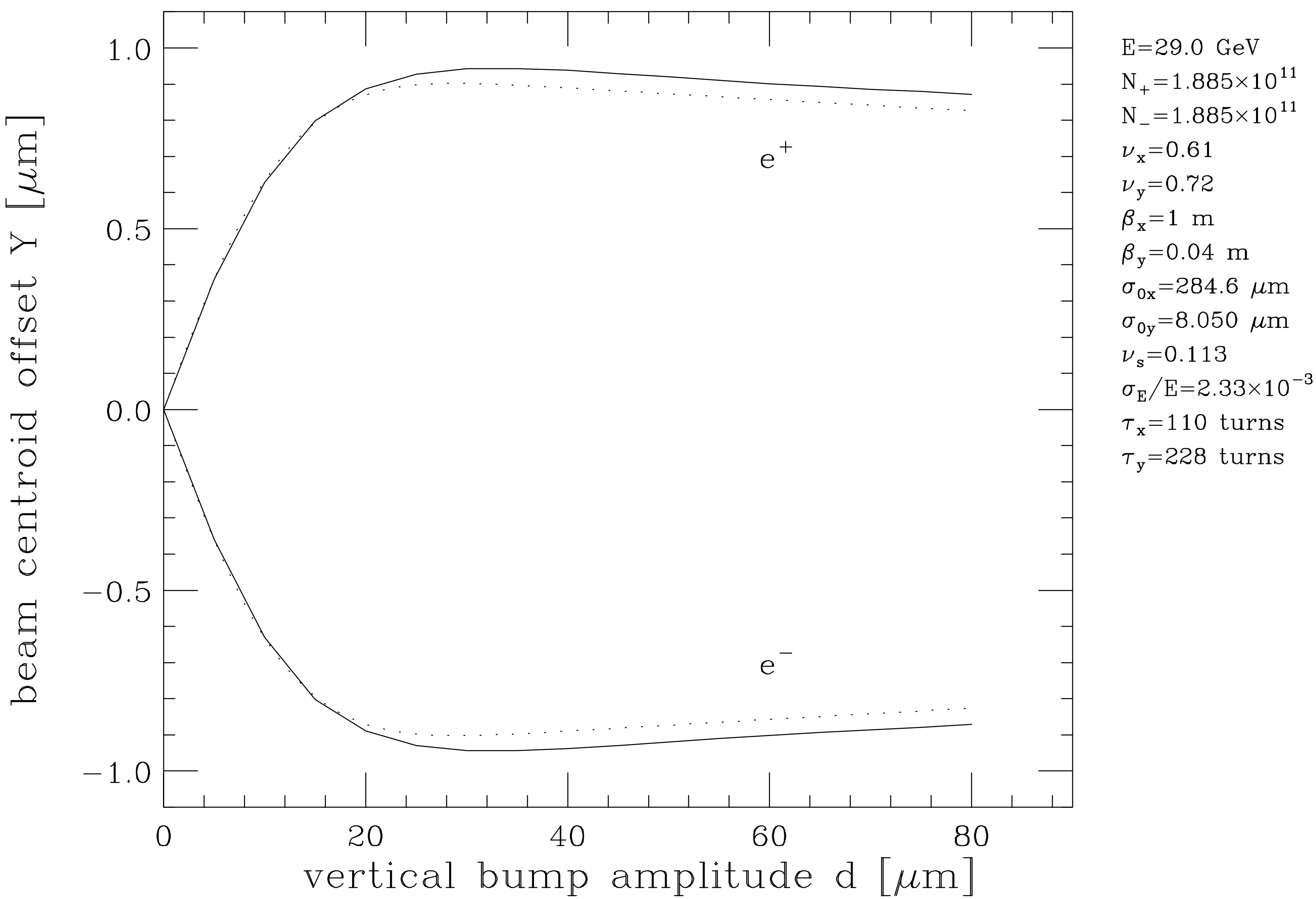

Fig. 21. Dependence of beam centroid offset on bump amplitude for TRISTAN. The two sets of curves correspond to the the full simulation using Yokoya's code (solid), and the analytical results from Eqs. (2.10) using the nominal beam sizes (dotted).

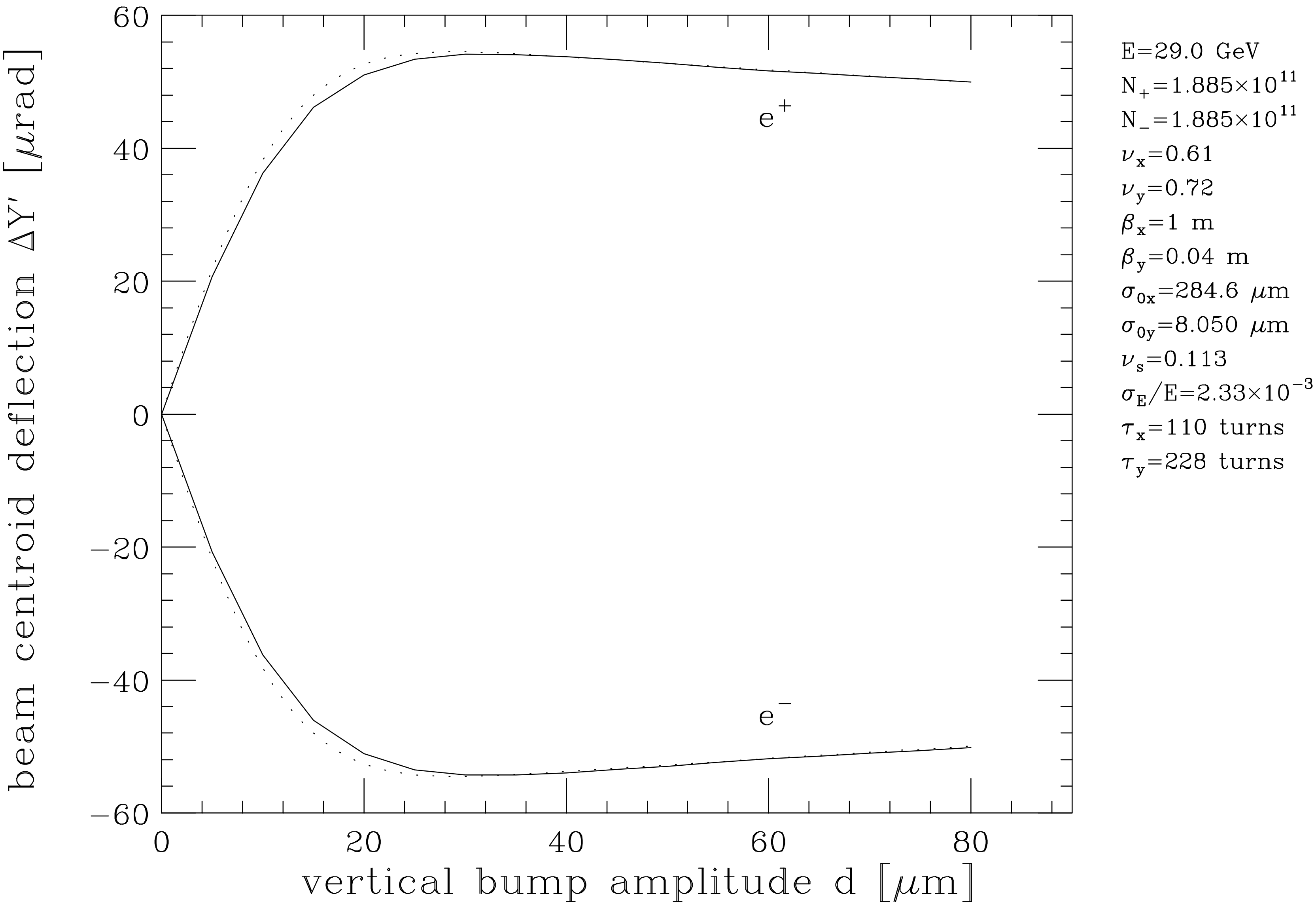

Fig. 22. Dependence of beam centroid deflection on bump amplitude for TRISTAN (Yokoya's code). The two sets of curves parallels those in Fig. 21.